IEEE Access
Multidisciplinary | Rapid Review | Open Access Journal

IEEE POWER & ENERGY SOCIETY SECTION

Received December 4, 2019, accepted December 19, 2019, date of publication December 27, 2019,
date of current version January 27, 2020.

Digital Object Identifier 10.1109/ACCESS.2019.2962620

A Modular Multiple DC Transformer Based DC Transmission System for PMSG Based Offshore Wind Farm Integration

PENGFEI HU[1], (Member, IEEE), RUI YIN[2], ZHENGXU HE[3], AND CONGLING WANG[4]
[1]College of Electrical Engineering, Zhejiang University, Hangzhou 310027, China
[2]State Grid Hebei Electric Power Company, Ltd., Shijiazhuang 050021, China
[3]Sichuan Energy Internet Research Institute, Tsinghua University, Chengdu 610213, China
[4]School of Mechanical and Electrical Engineering, University of Electronic Science and Technology of China, Chengdu 611731, China

Corresponding author: Pengfei Hu (hupengfei01@163.com)

ABSTRACT In this paper, a modular multiple DC (MMDC) transformer based DC transmission system, which is used for permanent magnetic synchronous generator (PMSG) based offshore wind farm grid connection, is proposed. The MMDC transformer is composed of input-parallel output-series (IPOS) DC/DC submodule groups, each of which consists of several input-series output-series (ISOS) LLC resonant converters (i.e., submodules). In the offshore wind farm, the electrical power generated by PMSG is converted to DC power by diode rectifier. Compared with the existing offshore wind farm grid-connection schemes, the proposed system has advantages of fewer conversion stages, higher efficiency and lower cost. The mathematical relationship of the system is studied, and then one kind of control strategy is proposed. Furthermore, a detailed DC transmission system simulation model containing a 160 submodules (LLC resonant converters) based MMDC transformer is built in PSCAD/EMTDC. Finally, a down-scaled experimental prototype of the DC system, which includes 9 submodules, is presented. Both simulation and experimental results validate the feasibility of the proposed DC system and effectiveness of the control strategy.

INDEX TERMS Offshore DC wind farm, modular multiple DC transformer, HVDC, input-parallel output-series, input-series output-series.

Nomenclature

The group number and submodule number of the MMDC are denoted with the subscript "i" and "j", respectively. The following symbols appear in the text or the figures.

P_{in_ij}	Input power of the jth submodule in the ith group
V_{in_ij}	Input voltage of the jth submodule in the ith group
V_{o_ij}	Output voltage of the jth submodule in the ith group
V_{in}	Voltage of the medium voltage direct current (MVDC) bus
I_{in}	Output current of the diode based converter
I_{in_i}	Input current of the ith group
I_{in_ij}	Input current of the jth submodule in the ith group
f_{ref_ij}	Working frequency reference of the jth submodule in the ith group
V_{smref}	Input voltage reference of the jth submodule in the ith group
ω_r	Rotational speed of the rotor of the wind turbine
P_{ref}	Power reference generated by ω_r
P_{ref_g}	Power reference of each group
$\boldsymbol{P_{in\_i}}$	Input power of the ith group

The associate editor coordinating the review of this manuscript and approving it for publication was Guangya Yang.

I. INTRODUCTION

As the most mature renewable energy source (RES), more than 500 GW of capacity has been installed until year 2019. Most of the capacity is onshore wind power. However, with the increasing development, the onshore wind power capacity would reach its limit. Gradually, the attention is turned to

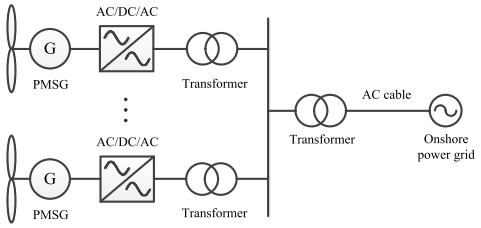

FIGURE 1. Offshore wind farm grid-connection scheme through HVAC.

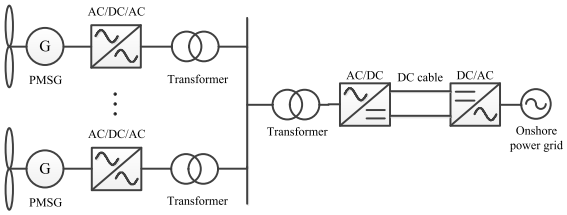

FIGURE 2. Offshore wind farm grid-connection scheme through conventional HVDC.

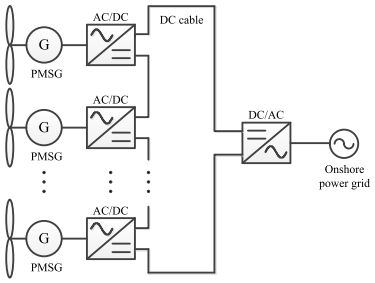

FIGURE 3. Serial-connection voltage step-up scheme for offshore wind farm.

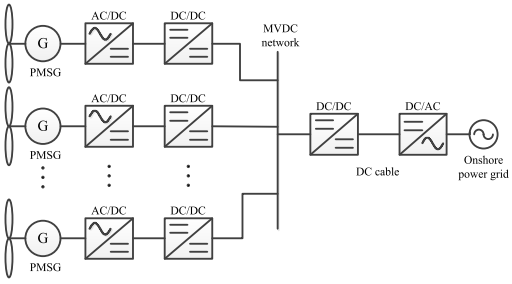

FIGURE 4. Two-stage DC voltage step-up topology for offshore wind farm.

the offshore wind energy source [1]. Generally, there are mainly two types of grid-connection schemes for offshore wind farm: i.e., high voltage alternative current (HVAC) system and high voltage direct current (HVDC) system. If the offshore wind farm is not far from mainland, HVAC based grid-connection scheme is better. Permanent magnet synchronous generator (PMSG) is taken as an example, the circuit topology consists of full-scale AC/DC/AC converter, medium-voltage fundamental-frequency transformers and high-voltage fundamental-frequency transformer, as shown in Fig.1. As for offshore wind farms located far away from mainland, the DC scheme would be more suitable, because the capacitance effect of the AC cable has more significant impact on the power transmission with the distance increasing. Generally, 50km offshore distance is regarded as a threshold. If offshore wind farms locate more than 50km away from the mainland, HVDC scheme seems to be the only option [2], [4]–[6].

There are two typical types of HVDC systems, i.e., line commutated converter (LCC) based HVDC and voltage source converter (VSC) based HVDC. Specifically, the modular multilevel converter (MMC) based HVDC is becoming the most popular topology out of the VSC based HVDC systems [7]–[13]. The topologies of the two schemes are illustrated in Fig.2, where the LCC based HVDC requires an extra stationary static synchronous compensators (STATCOM) used to regulate the AC bus voltage on the offshore side. As well, there are many stages in the DC scheme, including full-scale AC/DC/AC converter, medium-voltage fundamental-frequency transformers, high-voltage fundamental-frequency transformer, high-voltage DC/AC converter and STATCOM (only in LCC based HVDC). Compared with the LCC based HVDC, the VSC based HVDC has several advantages: (1) reduced devices and footprint, which is very suitable for the offshore application; (2) active and reactive power decoupled control characteristics. However, although the VSC based HVDC seems suitable for offshore wind farm integration, it still has the following drawbacks:

(1) Many power conversion stages are included in the system, which lowers overall efficiency and reliability of the system.

(2) Bulky fundamental-frequency transformers are used in the medium voltage AC (MVAC) system for wind energy collection. Unlike the onshore wind farm, offshore devices including transformers have to be placed on custom-built offshore platforms, which would be very expensive with large footprint.

Hence, to address these issues and improve the efficiency and economical performance, some new approaches for the offshore wind farm integration have been investigated. Some scholars proposed to use different types of HVDC converters for the grid-connecting of offshore wind farms, and their control strategies were studied as well. Diode rectifier, LCC, two-level VSC, MMC and their mixed structures have been studied in [2], [14]–[18]. These topologies all need to use the MVAC system to collect the electrical power, which means that the medium-voltage transformer is always needed. In addition, the MVAC system has large loss when it is used for offshore wind power farms. To resolve the issues caused by the MVAC system, offshore DC system was investigated by many scholars recently. In terms of the DC voltage step-up methods, there are mainly two categories: (1) boost the DC voltage through serial connecting wind turbines (see Fig.3) [19]–[23]; (2) utilize the step-up DC/DC converter (see Fig.4) [24]. Although the wind turbine serial-connection

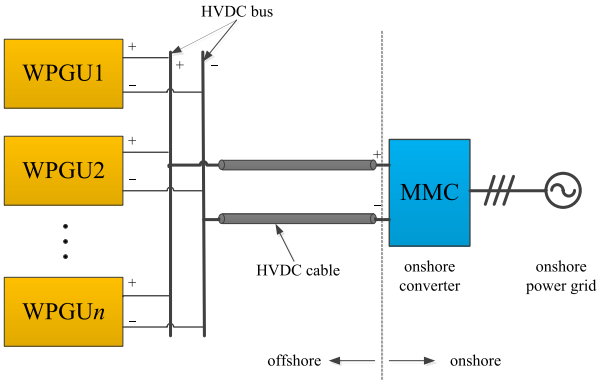

(a) Overall topology of the offshore wind power DC system

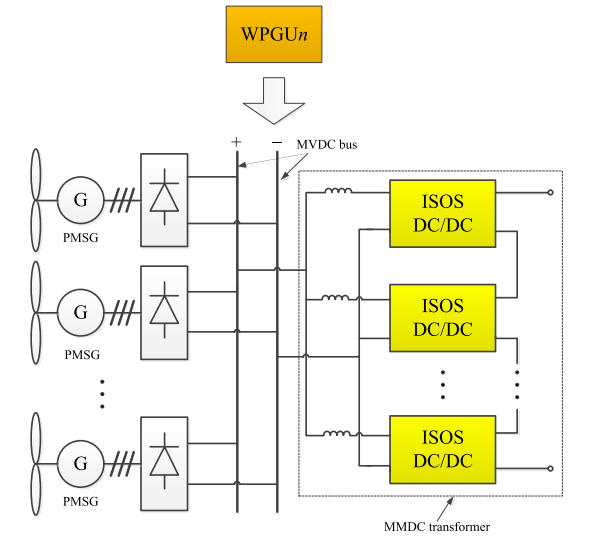

(b) Configuration of the MMDC transformer based WPGU

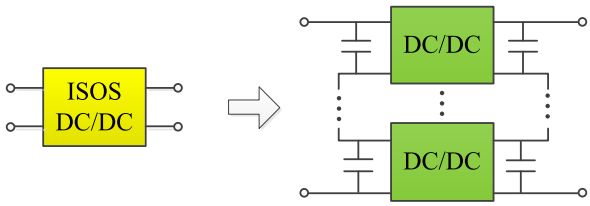

(c) Series-input series-output DC/DC converter

FIGURE 5. The proposed modular multiple DC/DC transformer based offshore DC system.

voltage step-up scheme looks simpler, the insulation for the top wind turbine is a big challenge. On the other hand, the step-up DC/DC converter based DC offshore wind farm is more realistic and has been paid much attention. Reference [25] investigated different control strategies of the DC offshore wind farms with the step-up DC/DC converters. Reference [26] applied fuzzy logic control to the DC offshore wind farm, which still has many conversion stages. To further reduce the conversion stages and footprint of the offshore DC system, this paper proposes a novel modular multiple DC/DC transformer based offshore DC system, shown in Fig.5, which utilizes only one stage DC step-up converter. The overall efficiency and volume could be reduced. In this paper, the PMSG based offshore wind farm is taken into consideration. Additionally, this paper also introduces control strategy of the proposed system, which could realize both the voltage and current balance of the submodules of the MMDC and the maximum power point tracking (MPPT) of the PMSG. Finally, a 160 DC/DC submodules based MMDC simulation model constructed in PSCAD/EMTDC, and a 9 DC/DC submodules based MMDC laboratory prototype are presented in this paper.

The rest of the paper is organized as follow: Section II presents the configuration and operating principles of the system; the control strategy is proposed in section III; simulation verification is presented in section IV; downscaled prototype of the system and the experimental results are presented in section V; conclusions are drawn in section VI.

II. CONFIGURATION AND OPERATING PRINCIPLES

A. CONFIGURATION OF THE PROPOSED SYSTEM

The proposed Modular Multiple DC (MMDC) transformer based DC transmission system for PMSG based offshore wind farm integration is shown in Fig.5 (a), which consists of one or several offshore wind power generation units (WPGU), an onshore modular multilevel converter (MMC), HVDC bus and cables. Each WPGU comprises one or several PMSGs (each comprising a diode rectifier), a medium voltage DC (MVDC) bus and an MMDC transformer, as shown in Fig.5 (b). As the key equipment of the proposed system, the MMDC transformer comprises several input-series output-parallel (ISOP) DC conversion groups, each of which consists of several input-series output-series (ISOS) DC/DC converter submodules, as shown in Fig.5 (c). The multiple series and parallel connection configuration increases the withstanding voltage and flowing-through current of the MMDC transformer, making it suitable for high-voltage and high-power applications, such as offshore wind power integration.

B. TOPOLOGY SELECTION OF MODULAR DC/DC CONVERTER

For the PMSG and diode rectifier based offshore wind farm integration application, the main features are high voltage and high power, unidirectional power transfer and output voltage variation. Therefore, the DC/DC submodule needs to satisfy the following requirements: (1) galvanic isolation between the low-voltage and high-voltage sides; (2) wide input voltage range, because output voltage of the diode-rectifier varies along with the input wind power; (3) undirectional power transfer of the DC/DC converter for the sake of economic performance. Thus, three topologies are selected as candidates, which are single active bridge (SAB) converter [27], LLC resonant converter [28] and LCC resonant converter [29]. Among the three types of converters, SAB converter and LCC converter have relatively high efficiency in the conventional offshore DC wind farm system. The LLC resonant converter

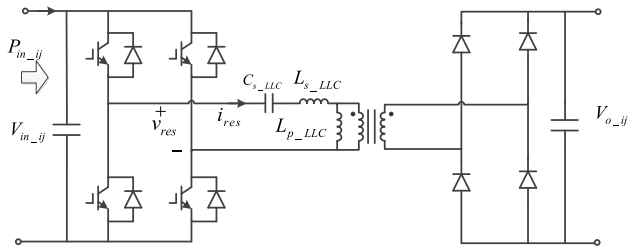

FIGURE 6. Topology of LLC resonant converter.

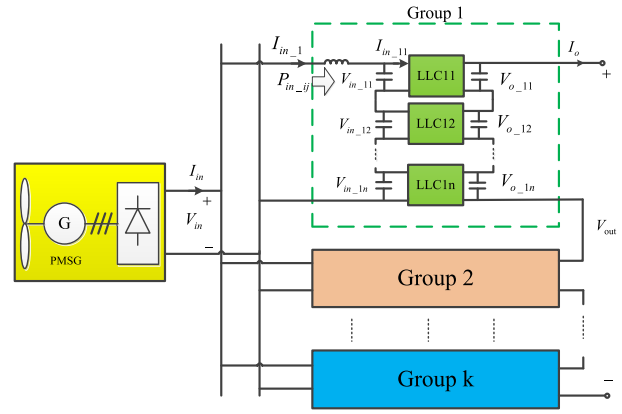

FIGURE 7. Sending side of the proposed system.

has some significant advantages: such as zero-voltage turn-on and zero-current turn-off, wide input voltage range, high efficiency under wide power range and so forth [30]–[32]. Since the PMSGs directly connect to the MVDC bus through diode rectifier, the voltage of the MVDC bus varies according to the input power of PMSGs (i.e., the wind speed). Thus, the input voltage of the MMDC has a relatively large voltage range, which makes the LLC resonant converter more suitable for this application.

The topology of the LLC resonant converter is shown in Fig.6. Operating principles of the LLC resonant converter have been comprehensively investigated by the literature [33]–[35]. Thus, details of the LLC operating principles would not be repeated in this paper.

C. MATHEMATICAL MODEL

The sending side of the proposed system is composed of PMSG, diode rectifier and MMDC, which is shown in Fig.7 (one PMSG unit is taken as an example). The mathematical relationship between the wind turbine and the MMDC is essential for the design of the control system.

The mathematical model of the wind turbine is expressed as

$$\lambda = \omega_r R/v \tag{1}$$

$$\lambda_i = \frac{1}{1/(\lambda + 0.08\beta) - 0.035/(\beta^3 + 1)} \tag{2}$$

$$C_p = 0.22(116/\lambda_i - 0.4\beta - 5)e^{-12.5/\lambda_i} \tag{3}$$

$$P_m = 0.5\rho\pi R^2(\frac{R}{\lambda})^3 C_p \omega_r^3 \tag{4}$$

$$T_m = P_m/\omega_r \tag{5}$$

where λ denotes the tip speed ratio, ω_r denotes the rotational speed of the rotor, R denotes the radius of the blade, β denotes the pitch angle, C_p denotes the wind-power utilization factor, P_m denotes the output mechanical power and T_m denotes the mechanical torque. Combing eqns. (1) to (4) yields

$$P_m = k_{opt}\omega_r^3 \tag{6}$$

where k_{opt} denotes the optimal coefficient which makes the wind turbine generates the maximum power on the conditions of various wind speeds. On the other hand, the mathematical model of the PMSG can be illustrated as

$$P_G = V_{in}I_{in} \tag{7}$$

$$T_e = P_G/\omega_r \tag{8}$$

$$J\frac{d\omega_r}{dt} = T_m - T_e \tag{9}$$

$$e_s = n_p\omega_r\psi_f \tag{10}$$

where P_G denotes electromagnetic power generated by the PMSG, T_e denotes electromagnetic torque, J denotes rotational inertia, e_s denotes the excitation electromotive force, n_p denotes pole pairs, and ψ_f denotes the flux linkage. Regarding the synchronous reactance of the PMSG as the commutation reactance of the diode rectifier, the output voltage of the DBC can be obtained as [36]

$$V_{in} = \frac{6\sqrt{3}}{\pi}e_s - \frac{6n_p\omega_r L_s}{\pi}I_{in} \tag{11}$$

where L_s is the synchronous reactance.

Ignoring the loss of the PMSG, the output power of the PMSG should be equal to the input power, which is

$$P_G = V_{in}I_{in} = P_m = k_{opt}\omega_r^3 \tag{12}$$

For the MMDC, the input power (P_G), which is generated by the maximum power point track (MPPT) strategy should be equally shared by each submodule. Thus, given that the MMDC consists of k submodule groups, and each group consists of n submodules, the input power of each submodule can be calculated by

$$P_{in\_ij} = N_w P_G/(kn) \tag{13}$$

where N_w denotes the PMSG count in a WPGU. Combing eqns. (10), (12) and (13) yields

$$P_{in\_ij} = \frac{N_w k_{opt}}{nkn_p^3\psi_f^3}e_s^3 \tag{14}$$

Additionally, combing eqns. (10), (11) and (12) yields

$$V_{in} = \frac{1}{2}(A + \sqrt{A^2 - 4Be_s^2})e_s \tag{15}$$

where $A = \frac{6\sqrt{3}}{\pi}$, $B = \frac{6k_{opt}L_s}{\pi n_p^3\psi_f^4}$. Thus, the input voltage of the jth submodule in the ith group can be written as

$$V_{in\_ij} = \frac{1}{2n}(A + \sqrt{A^2 - 4Be_s^2})e_s \tag{16}$$

TABLE 1. Economical efficiency comparison.

	Topology 1	Topology 2	Proposed Topology
AC/DC converter	$2nS$	nS	nS
DC/AC converter	nS	0	0
DC/DC converter	0	$2nS$	nS
Fundamental frequency transformer	need	/	/
Medium frequency transformer	/	need	need
Offshore platform	need	need	/

Hence, according to eqns. (13) and (16), the input voltage and power of the LLC submodule are dependent on the excitation electromotive force (e_s).

D. COST ANALYSIS

To clarify the economical efficiency of the proposed topology, two other feasible solutions (presented in Figure 2 and Figure 4) are used to compare with the proposed topology. For the sake of simplicity, the topologies shown in Figure 2 and Figure 4 are named topology 1 and topology 2, respectively. Since many different AC/DC and DC/DC topologies could be employed, it is difficult to comprehensively compare the power switch count and corresponding loss. Capacity of each wind turbine is supposed as S, and the total number of wind turbines is selected as n. It is worth mentioning that the AC/DC/AC converter in topology 1 is regarded as a AC/DC converter plus a DC/AC converter. Thus, the power capacity of converter is employed as the surrogate index. Other aspects including the fundamental frequency transformer, medium frequency transformer and offshore platform are disscussed as well. The detailed comparison results are depicted in Table 1, where it can be seen that the proposed topology only has nS power capacity of converters and does not need offshore platform. It can be concluded that the economical efficiency of the proposed topology is better than other two topologies.

III. CONTROL SYSTEM

A. OPERATING CURVE OF THE LLC SUBMODULE

Since the LLC resonant converter is selected as the DC/DC submodule of the MMDC, the operating curve of the LLC is needed for the design of the control system. Generally, the voltage gain of the LLC is expressed as [37]

$$M = \frac{V_{o\_ij}}{n_t V_{i\_ij}} = \left| \frac{(\frac{\omega^2}{\omega_o^2})\sqrt{m(m-1)}}{(\frac{\omega^2}{\omega_p^2}-1)+j(\frac{\omega}{\omega_o})(\frac{\omega^2}{\omega_o^2}-1)(m-1)Q^e} \right| \quad (17)$$

where M denotes the voltage gain, V_{o_ij} denotes the output voltage of the jth submodule in the ith group, n_t denotes the

TABLE 2. Parameters of the LLC resonant converter.

Items	Value
Rated output DC voltage	2.5 kV
Input DC voltage	0.39 ~ 1 kV
Input power	8 ~ 250 kW
Working frequency	3.01 ~ 5.17 kHz
Input capacitance	250 μF
Output capacitance	100 μF
Series capacitance (C_{s_LLC})	9.2 μF
Series inductance (L_{s_LLC})	76.2 μH
Parallel inductance (L_{p_LLC})	381.1 μH

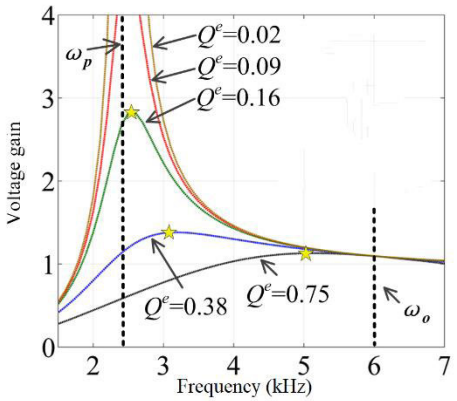

FIGURE 8. Curve of voltage gain-frequency characteristic.

voltage ratio of the medium frequency transformer, ω denotes the angular frequency of the submodule, ω_o and ω_p denote the resonant angular frequencies determined by the resonant elements L_{s_LLC}, C_{s_LLC} and L_{p_LLC}, which are shown in Fig.6. m denotes the ratio of $L_{p\_LLC} + L_{s\_LLC}$ to L_{s_LLC}. Q_e denotes the equivalent quality factor determined by the parameters and input power, shown as [37]

$$Q^e = \sqrt{\frac{L_{s\_LLC}}{C_{s\_LLC}}} \frac{\pi^2 m}{8n_t^2(m-1)V_{o\_ij}^2} P_{in\_ij} \quad (18)$$

where P_{in_ij} denotes the input power of the jth submodule in the ith group. According to the eqns.(17), (18) and parameters in Table 2, the voltage gain-frequency characteristic curve on the condition of $f_0 = 6$ kHz (f_0 is the corresponding frequency of ω_o) and $m = 6$ can be expressed as Fig.8, which shows that both Q_e and f have impact on voltage gain. Assuming that the onshore MMC regulates the DC voltage of high-voltage side as a constant, and the submodule output voltages are balanced well, and PMSGs connect to the MVDC via diode rectifiers, the input voltage of the MMDC varies following the excitation electromotive force of the wind turbine. Thus, according to eqns. (16) and (17), the submodule voltage gain is dependent on the excitation electromotive force of PMSG (e_s). In the meantime, the Q_e is also dependent on the input power, see eqn. (19), which is a function of e_s. Hence, the operating points shift among the voltage gain-frequency curves with the varying e_s (i.e. varying

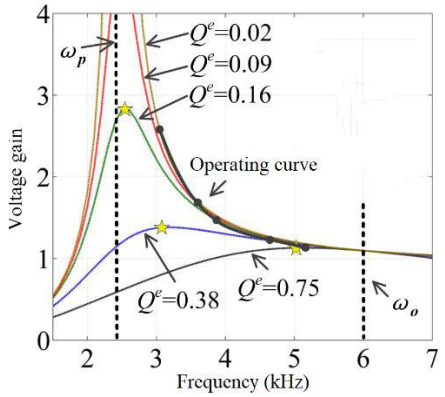

FIGURE 9. Operating curve of the LLC resonant converter.

wind speeds). The operating curve can be obtained by connecting these operating points together.

To obtain the submodule operating curve, submitting eqn. (14) into eqn. (18) yields

$$Q^e = \frac{\pi^2 m N_w k_{opt}\sqrt{L_{s\_LLC}C_{s\_LLC}}}{8n_t^2(m-1)V_{o\_ij}^2 nkn_p^3\psi_f^3 C_{s\_LLC}}e_s^3 = Ce_s^3 \quad (19)$$

where

$$C = \frac{\pi^2 m N_w k_{opt}\sqrt{L_{s\_LLC}C_{s\_LLC}}}{8n_t^2(m-1)V_{o\_ij}^2 nkn_p^3\psi_f^3 C_{s\_LLC}}$$

Then, submitting eqn. (16) into eqn. (17) yields

$$M = \frac{V_{o\_ij}}{n_t^2 V_{i\_ij}} = \frac{2N_{sm}V_{o\_ij}}{(A+\sqrt{A^2-4Be_s^2})n_t e_s} \quad (20)$$

In eqns. (19) and (20), A, B and C all are constants. Each e_s has a corresponding M and Q_e. Additionally, to ensure soft switching of IGBTs and zero recovery loss of diodes, the operating points should locate between the ω_p and ω_0 [28]. By selecting a set of e_s in the value range and calculating the corresponding M and Q_e, the operating curve of the submodule can be obtained as Fig.9.

B. CONTROL STRATEGY

To ensure the proposed system working normally, three main control goals need to be reached: (1) MPPT of PSMGs; (2) input currents balance between the submodule groups; (3) input voltages balance of submodules in the same group. According to the operating curve in Fig.9, the voltage gain (M) is a decreasing function of working frequency (f), so the input voltage of submodule could be regulated by adjusting the working frequency. Additionally, the input current of submodule (I_{in_ij}) would be taken as the inner loop feedback variable to improve the dynamic characteristic of the control loop. Thus, the submodule input voltage regulation loop is shown as Fig.10 (a). It is worth mentioning that the input voltage reference, which is denoted by V_{smref}, is the same, if each group contains the same submodule count. Another goal is to equally share the output currents of the diode rectifiers

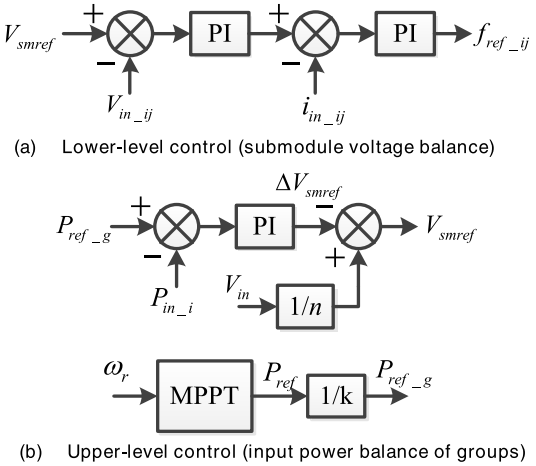

FIGURE 10. Two-level control strategies of the MMDC.

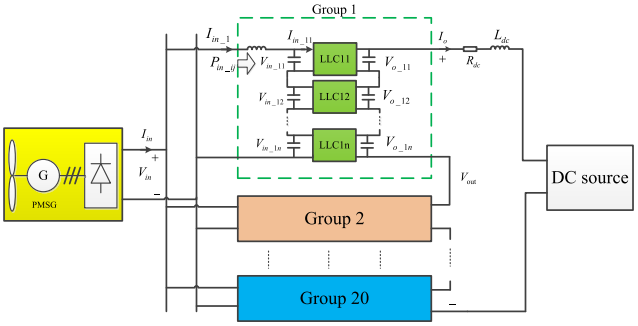

FIGURE 11. Circuit schematic diagram of simulation model.

between the submodule groups. Since the groups have the same input voltage (V_{in}), the current sharing is equivalent to the input power sharing. Thus, a regulator of input power of submodule groups is designed as Fig.10 (b), while this regulator generates the input submodule voltage reference. Moreover, the input power of submodule groups is generated by equally sharing of the output power of the wind turbine, which outputs the maximum power according to the wind speed, as shown in Fig.10 (b). The submodule voltage balance regulator needs to be implemented in each LLC submodule, i.e., there are $k \times n$ submodule voltage balance controllers, meanwhile there are k input power balance of groups regulators. Hence, it is reasonable to deploy the voltage balance regulators in the lower-level controller, while the power balance regulators in the upper-level controller. In addition, the onshore MMC employs the conventional dq-decoupled control to regulate the HVDC bus voltage, which is not shown here anymore.

IV. SIMULATION VERIFICATION

To verify the feasibility of the proposed system, a simulation model as shown in Fig.11, which includes a WPGU, a high-voltage cable and a DC source, is constructed in the PSCAD/EMTDC software environment. To precisely

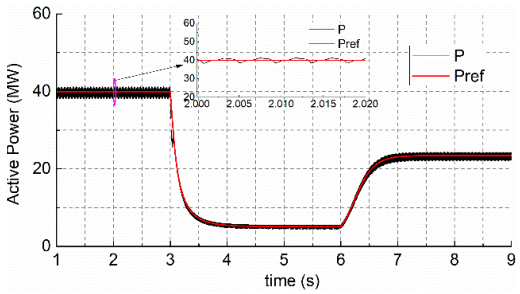

(a) Active power reference and real value

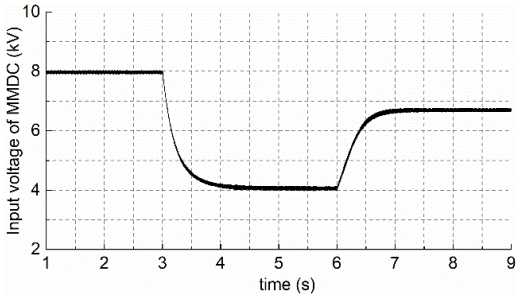

(b) Input voltages of MMDC transformer

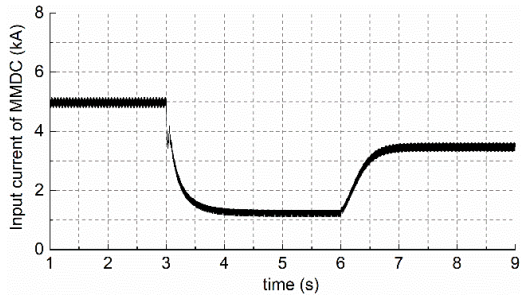

(c) Input current of MMDC transformer

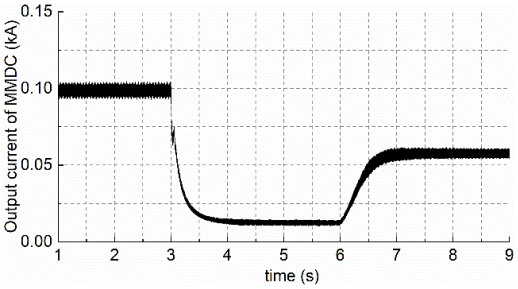

(d) Output current of MMDC transformer

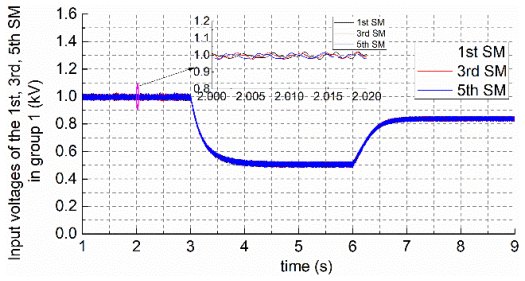

(e) Input voltages of the 1st, 3rd and 5th submodules in group 1

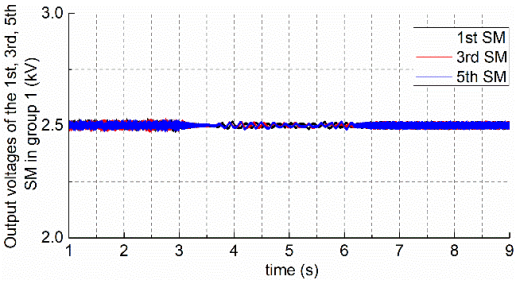

(f) Output voltages of the 1st, 3rd and 5th submodules in group 1

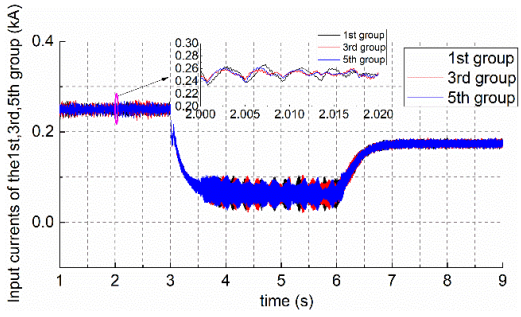

(g) Input currents of the 1st, 3rd and 5th groups

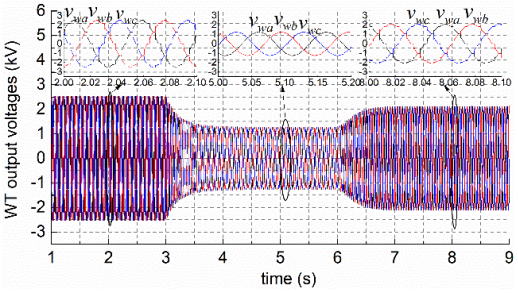

(h) Output voltages of the PMSG

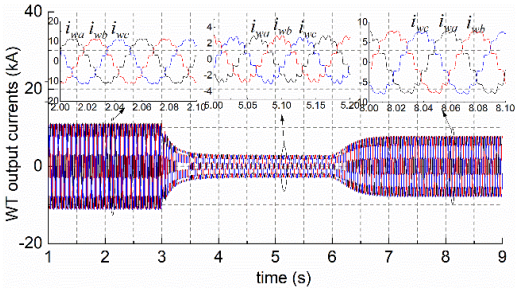

(i) Output currents of the PMSG

FIGURE 12. Steady-state and transient-state of the proposed system.

TABLE 3. Parameters of the MMDC in simulation.

Items	Symbol	Value
Rated output DC voltage	U_{dcout}	400 kV
Rated input DC voltage	U_{dcin}	8 kV
Rated power	P	40 MW
Group number of sub-modules	k	20
Submodule count of each group	n	8
Total number of sub-modules	N_{sum}	160
Input inductance	L_0	100 μH

TABLE 4. Parameters of PMSG and HVDC cable in simulation.

	Items	Symbol	Value
PMSG	Base value of power	P_b	8 MW
	Base value of voltage	V_b	2.96 kV
	Base value of frequency	f_b	20 Hz
	Rated power	P_{wt}	40 MW
	Rated voltage	U_{wt}	2.96 kV
	Rated frequency	f_{wt}	20 Hz
	Pole pairs	M	150
	Unsaturated reactance of d axis	X_d	0.7 pu
	Unsaturated reactance of q axis	X_q	0.7 pu
	Damper winding reactance of d axis	X_{kd}	0.62 pu
	Damper winding reactance of q axis	X_{kq}	0.62 pu
	Magnetic strength	ϕ	1.0 pu
HVDC cable	Equivalent resistance	R_{dc}	3.4 ohm
	Equivalent inductance	L_{dc}	12 mH

simulate the high-voltage high-power working condition in the offshore application, an MMDC model containing 160 LLC resonant converters has been built. These submodules are divided into 20 groups, each of which consists of 8 submodules. To simplify the simulation model, only one WPGU is employed, and the onshore MMC is simplified as a DC source with rated voltage 400kV. The rated input and output voltages of the MMDC are 8kV and 400kV, respectively. The rated input and output voltages of each LLC resonant converter are 1kV and 2.5kV, respectively. Thus, the step-up gain of the MMDC reaches 50. Other parameters of the MMDC are illustrated in Table 3 and 4.

To validate the performance of the MMDC under the condition of wind speed variation. The transient-state process is designed as follow: at $t = 3$s, wind speed reduces from 12 m/s to 6 m/s, and then maintains 6 m/s for 3s, finally, rises to 10 m/s.

Fig. 12 shows the system performance during this simulation process. Fig.12(a) illustrates that the power reference varies according to the wind speed, meanwhile the actual output power tracks the power reference quickly and stably. Fig.12(b) and (c) show that the input voltage and current of the MMDC transformer response to the step change of wind speed quickly and stably, as analyzed before. Through the MMDC transformer, the output current behaves stable, shown in Fig.12(d). Fig.12 (e) and (f) show the input and output voltages of the 1st, 3rd, and 5th submodules in group 1,

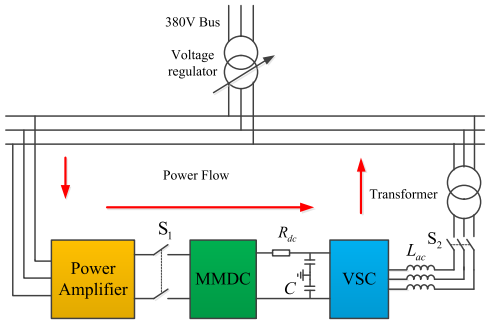

FIGURE 13. Circuit schematic diagram of the experimental system.

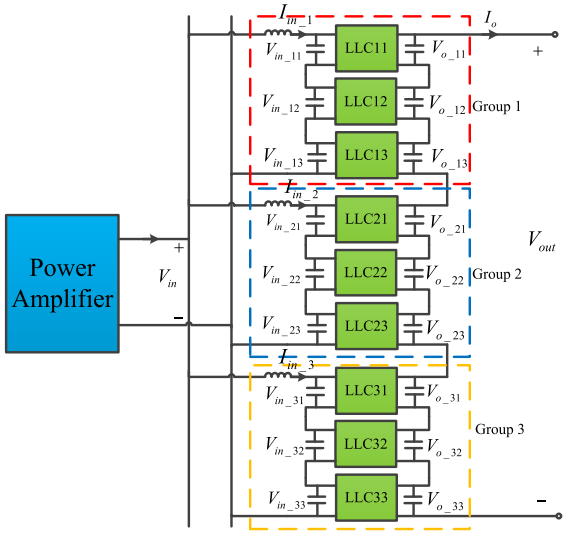

FIGURE 14. Circuit schematic diagram of the MMDC in the experimental setup.

TABLE 5. Parameters of the MMDC in experiment.

Items	Value
Rated output DC voltage	750 V
Rated input DC voltage	135 V
Rated power	1 kW
Group number of sub-modules	3
Sub-module number of each group	3
Total number of sub-modules	9
Input inductance	1 mH

which are well balanced and stable. The ripples of these voltages are only 1% of the rated value. Deserved to be mentioned, voltages of all submodules are balanced well and the three submodules in group 1 are selected as representatives. Fig.12 (g) shows that the input currents of the 1st, 3rd, and 5th groups are selected well balanced during the transient process. Fig.12 (h) and (i) depict the output voltages and currents of the PMSG. Overall, the simulation results validate the feasibility of the proposed system and the effectiveness of the control strategy.

TABLE 6. Parameters of sub-modules.

Items	Value
Rated output DC voltage	83.3 V
Rated input DC voltage	45 V
Rated working frequency	50 kHz
Voltage ratio	1:1.8
Input capacitance	100 μF
Output capacitance	940 μF
Series resonance capacitance	0.68 μF
Series resonance inductance	15 μH
Parallel resonance inductance	96 μH

TABLE 7. Parameters of the power amplifier.

Items	Value
Frequency range	DC~20kHz
Working modes	DC constant voltage DC constant current AC constant voltage AC constant current
Maximum output voltage	200V(DC); 141V(AC)
Rated power	2.55 kW(DC); 2 kVA(AC)
Gain	Constant voltage: 100 V/V Constant current: 12 A/V

V. EXPERIMENTAL RESULTS

To further verify the proposed topology and control strategy, a down-scaled MMDC transformer based DC transmission system is built in laboratory. The WPGU is modelled by a power amplifier, and the onshore MMC is represented by a two-level VSC. Due to the limitation of experimental conditions, only one WPGU is deployed in the system. The circuit schematic diagram of the down-scaled system is depicted in Fig.13, where the power is drawn from the distribution network and then feeds back to it. The key element of the system is the MMDC transformer, which consists of three groups and each group comprises three LLC resonant converters in the experimental setup, shown in Fig.14. The voltage variables and current directions are depicted in Fig.14 as well, which makes it easier to understand the experimental results. Then, the photo of the experimental setup is shown in Fig.15. Parameters of the down-scaled experimental system are illustrated in Table 5 to 7.

The wind speed step test is designed to examine the transient-state performances of the system. As seen in Fig.13, the DC voltage of the high-voltage side is regulated by the VSC, which is set to 750V. At the beginning, the wind speed is 9 m/s; from t = 30s on, the wind speed steps up to 10 m/s; and then it steps down to 8 m/s at t = 70s. Fig.16 and 17 illustrate performances of the MMDC prototype during this test. Fig.16(a) shows that the input voltages of the first sub-modules of the three groups are balanced well during both the steady state and transient state. Fig.16(b) illustrates that the output voltages of the three sub-modules are also balanced well with little difference, which can be ignored. And the output voltages keep constant during the whole procedure.

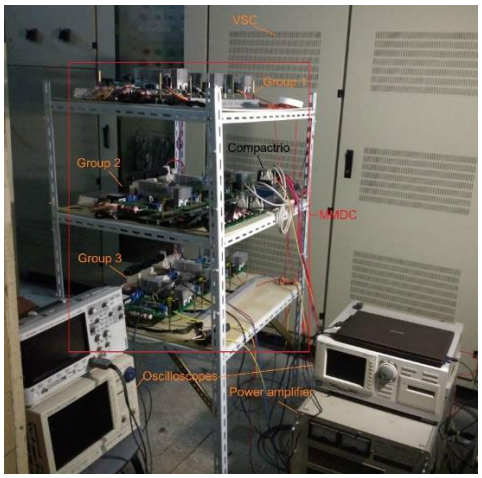

FIGURE 15. The photo of the experimental setup.

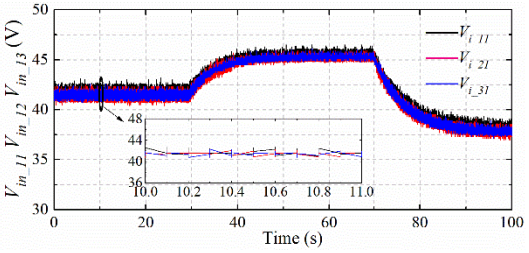

(a) Input voltages of the first sub-modules in group 1 to group 3

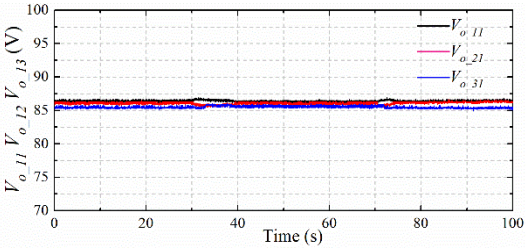

(b) Output voltages of the first sub-modules in group 1 to group 3

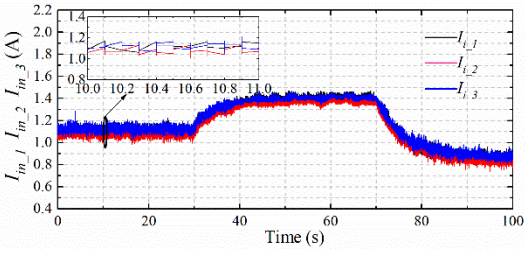

(c) Input currents of group 1 to group 3

FIGURE 16. Voltage and current sharing performances of the MMDC prototype.

Fig.16(c) shows that the input currents of the three groups are also balanced well. The three figures validate the effectiveness of the proposed voltage balancing and current balancing control strategy. In addition, the input power, input voltage and output voltage of the MMDC are depicted in Fig.17,

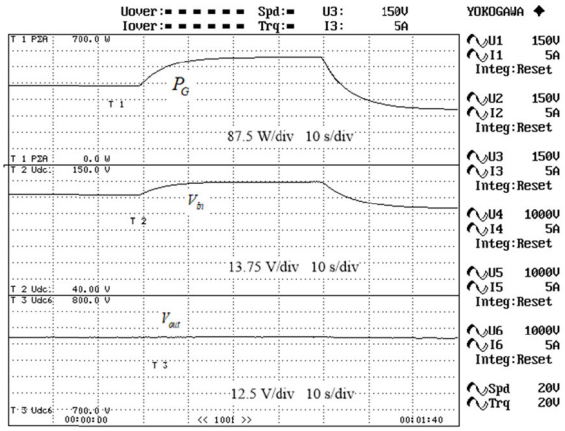

FIGURE 17. **Input power, input and output voltages of the MMDC transformer prototype.**

which shows that the input and output characteristics meet the design values.

VI. CONCLUSION

In this paper, a modular multiple DC transformer based DC transmission system, which has the characteristics of high efficiency, low cost and high reliability, for PMSG based wind farm integration is proposed. Mathematical relationship of the proposed system in comprehensively investigated. A two-level control strategy which could realize both MPPT for PMSG and voltage/current balance for MMDC transformer is proposed and verified. A detailed complicated simulation model is constructed and a down-scaled prototype is presented. Both simulation and experimental results validate the feasibility of the system and effectiveness of the control strategy.

ACKNOWLEDGMENT

The authors would like to express gratitude to Prof. D. Jiang for his proofreading and helpful suggestions.

REFERENCES

[1] Q. Wang, Z. Yu, R. Ye, Z. Lin, and Y. Tang, "An ordered curtailment strategy for offshore wind power under extreme weather conditions considering the resilience of the grid," *IEEE Access*, vol. 7, pp. 54824–54833, 2019.

[2] T. Kawaguchi, T. Sakazaki, T. Isobe, and R. Shimada, "Offshore-wind-farm configuration using diode rectifier with MERS in current link topology," *IEEE Trans. Ind. Electron.*, vol. 60, no. 7, pp. 2930–2937, Jul. 2013.

[3] S. V. Bozhko, R. Blasco-Gimnez, R. Li, J. C. Clare, and G. M. Asher, "Control of offshore DFIG-based wind farm grid with line-commutated HVDC Connection," *IEEE Trans. Energy Convers.*, vol. 22, no. 1, pp. 71–78, Mar. 2007.

[4] S. Bernal-Perez, S. Ano-Villalba, R. Blasco-Gimenez, and J. Rodriguez-D'Derlee, "Efficiency and fault ride-through performance of a diode-rectifier- and VSC-inverter-based HVDC link for offshore wind farms," *IEEE Trans. Ind. Electron.*, vol. 60, no. 6, pp. 2401–2409, Jun. 2013.

[5] P. Bresesti, W. L. Kling, R. L. Hendriks, and R. Vailati, "HVDC connection of offshore wind farms to the transmission system," *IEEE Trans. Energy Convers.*, vol. 22, no. 1, pp. 37–43, Mar. 2007.

[6] R. Yin, M. Shi, W. Hu, J. Guo, P. Hu, and Y. Wang, "An accelerated model of modular isolated DC/DC converter used in offshore DC wind farm," *IEEE Trans. Power Electron.*, vol. 34, no. 4, pp. 3150–3163, Apr. 2019.

[7] P. Hu, R. Teodorescu, S. Wang, S. Li, and J. M. Guerrero, "A currentless sorting and selection-based capacitor-voltage-balancing method for modular multilevel converters," *IEEE Trans. Power Electron.*, vol. 34, no. 2, pp. 1022–1025, Feb. 2019.

[8] F. Yan, P. Wang, X.-P. Zhang, J. Xie, X. Li, C. Tang, and Z. Zhao, "Coordinated start-up control and inter-converter oscillations damping for MMC-HVDC grid," *IEEE Access*, vol. 7, pp. 65093–65102, 2019.

[9] P. Hu, R. Teodorescu, and J. M. Guerrero, "Negative-sequence second-order circulating current injection for hybrid MMC under over-modulation conditions," *IEEE J. Emerg. Sel. Topics Power Electron.*, to be published, doi: 10.1109/jestpe.2019.2908828.

[10] F. Deng, Q. Heng, C. Liu, Q. Wang, R. Zhu, X. Cai, and Z. Chen, "Power losses control for modular multilevel converters under capacitor deterioration," *IEEE J. Emerg. Sel. Topics Power Electron.*, to be published.

[11] P. Hu, Z. He, S. Li, and J. M. Guerrero, "Non-ideal proportional resonant control for modular multilevel converters under sub-module fault conditions," *IEEE Trans. Energy Convers.*, vol. 34, no. 4, pp. 1741–1750, Dec. 2019.

[12] P. Hu, R. Teodorescu, and J. M. Guerrero, "State observer based capacitor-voltage-balancing method for modular multilevel converters without arm-current sensors," *Int. J. Electr. Power Energy Syst.*, vol. 113, pp. 188–196, Dec. 2019.

[13] P. Hu, Z. He, R. Yin, J. Guo, J. M. Guerrero, and R. Teodorescu, "Analysis and optimization of hybrid modular multilevel converters under over-modulation conditions," *Int. J. Elect. Power Energy Syst.*, vol. 116, Mar. 2020, Art. no. 105578, doi: 10.1016/j.ijepes.2019.105578.

[14] S. Bozhko, G. Asher, R. Li, J. Clare, and L. Yao, "Large offshore DFIG-based wind farm with line-commutated HVDC connection to the main grid: Engineering studies," *IEEE Trans. Energy Convers.*, vol. 23, no. 1, pp. 119–127, Mar. 2008.

[15] L. Xu, L. Yao, and C. Sasse, "Grid integration of large DFIG-based wind farms using VSC transmission," *IEEE Trans. Power Syst.*, vol. 22, no. 3, pp. 976–984, Aug. 2007.

[16] T. H. Nguyen, D.-C. Lee, and C.-K. Kim, "A series-connected topology of a diode rectifier and a voltage-source converter for an HVDC transmission system," *IEEE Trans. Power Electron.*, vol. 29, no. 4, pp. 1579–1584, Apr. 2014.

[17] Z. Lu, Y. Ye, and Y. Qiao, "An adaptive frequency regulation method with grid-friendly restoration for VSC-HVDC integrated offshore wind farms," *IEEE Trans. Power Syst.*, vol. 34, no. 5, pp. 3582–3593, Sep. 2019.

[18] Y. Chang and X. Cai, "Hybrid topology of a diode-rectifier-based HVDC system for offshore wind farms," *IEEE J. Emerg. Sel. Topics Power Electron.*, vol. 7, no. 3, pp. 2116–2128, Sep. 2019.

[19] H. Zhang, F. Gruson, D. M. F. Rodriguez, and C. Saudemont, "Overvoltage limitation method of an offshore wind farm with DC series-parallel collection grid," *IEEE Trans. Sustain. Energy*, vol. 10, no. 1, pp. 204–213, Jan. 2019.

[20] N. Holtsmark, H. J. Bahirat, M. Molinas, B. A. Mork, and H. K. Hoidalen, "An all-DC offshore wind farm with series-connected turbines: An alternative to the classical parallel AC model?" *IEEE Trans. Ind. Electron.*, vol. 60, no. 6, pp. 2420–2428, Jun. 2013.

[21] A. Garcés and M. Molinas, "Coordinated control of series-connected offshore wind park based on matrix converters," *Wind Energy*, vol. 15, no. 6, pp. 827–845, Sep. 2012.

[22] M. Guan, "A series-connected offshore wind farm based on modular dual-active-bridge (DAB) isolated DC–DC converter," *IEEE Trans. Energy Convers.*, vol. 34, no. 3, pp. 1422–1431, Sep. 2019.

[23] M. Guan and Z. Xu, "A novel concept of offshore wind-power collection and transmission system based on cascaded converter topology," *Int. Trans. Electr. Energy Syst.*, vol. 24, no. 3, pp. 363–377, Mar. 2014.

[24] W. Chen, A. Q. Huang, C. Li, G. Wang, and W. Gu, "Analysis and comparison of medium voltage high power DC/DC converters for offshore wind energy systems," *IEEE Trans. Power Electron.*, vol. 28, no. 4, pp. 2014–2023, Apr. 2013.

[25] P. Monjean, J. Delanoë, D. Marin, J. Auguste, C. Saudemont, and B. Robyns, "Control strategies of DC-based offshore wind farm," in *Proc. 14th Eur. Conf. Power Electron. Appl.*, Birmingham, U.K., Aug./Sep. 2011, pp. 1–9.

[26] S. M. Muyeen, A. Al-Durra, and J. Tamura, "Transmission of bulk power from DC-based offshore wind farm to grid through HVDC system," in *Wind Energy Conversion Systems* (Green Energy and Technology). S. Muyeen, Ed. London, U.K.: Springer, 2012.

[27] X. Wu, X. Xie, J. Zhang, R. Zhao, and Z. Qian, "Soft switched full bridge DC–DC converter with reduced circulating loss and filter requirement," *IEEE Trans. Power Electron.*, vol. 22, no. 5, pp. 1949–1955, Sep. 2007.
[28] B.-C. Kim, K.-B. Park, C.-E. Kim, B.-H. Lee, and G.-W. Moon, "LLC resonant converter with adaptive link-voltage variation for a high-power-density adapter," *IEEE Trans. Power Electron.*, vol. 25, no. 9, pp. 2248–2252, Sep. 2010.
[29] S. Mao, Y. Chen, C. Li, W. Li, J. Popovic, and J. A. Ferreira, "A coupled-inductor-based LCC resonant converter with the primary-parallel–secondary-series configuration to achieve output-voltage sharing for HV generator applications," *IEEE Trans. Power Electron.*, vol. 34, no. 7, pp. 6108–6122, Jul. 2019.
[30] X. Fang, H. Hu, J. Shen, and I. Batarseh, "An optimal design of the LLC resonant converter based on peak gain estimation," in *Proc. 27th Annu. IEEE Appl. Power Electron. Conf. Exposit. (APEC)*, Orlando, FL, USA, Feb. 2012, pp. 1286–1291.
[31] A. Bhat, "Analysis and design of a modified series resonant converter," *IEEE Trans. Power Electron.*, vol. 8, no. 4, pp. 423–430, Oct. 1993.
[32] G. Raju and S. Doradla, "An LCL resonant converter with PWM control-analysis, simulation, and implementation," *IEEE Trans. Power Electron.*, vol. 10, no. 2, pp. 164–174, Mar. 1995.
[33] B. Yang, F. Lee, A. Zhang, and G. Huang, "LLC resonant converter for front end DC/DC conversion," in *Proc. APEC 17th Annu. IEEE Appl. Power Electron. Conf. Exposit.*, Dallas, TX, USA, vol. 2, Jun. 2003, pp. 1108–1112.
[34] J. Lazar and R. Martinelli, "Steady-state analysis of the LLC series resonant converter," in *Proc. APEC 16th Annu. IEEE Appl. Power Electron. Conf. Exposit.*, Anaheim, CA, USA, Nov. 2002, pp. 728–735.
[35] X. Fang, H. Hu, Z. J. Shen, and I. Batarseh, "Operation mode analysis and peak gain approximation of the LLC resonant converter," *IEEE Trans. Power Electron.*, vol. 27, no. 4, pp. 1985–1995, Apr. 2012.
[36] R. Yin, D. Jiang, Y. Du, P. Hu, and Y. Liang, "A novel control strategy for offshore DFIG-based wind farm integrated through diode-rectifier-based HVDC transmission," *Int. Trans. Electr. Energy Syst.*, vol. 25, no. 12, pp. 3553–3572, Dec. 2015.
[37] L. Half-Bridge, "Half-bridge LLC resonant converter design using FSFR-series fairchild power switch (FPS)," Appl. Note AN-4151. Fairchild Semiconductor Corporation, Sunnyvale, CA, USA, 2007.

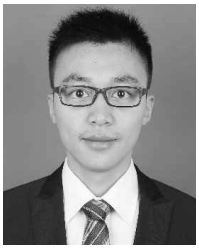

PENGFEI HU (Member, IEEE) received the B.E. and Ph.D. degrees in electrical engineering and its automation from the College of Electrical Engineering, Zhejiang University, Hangzhou, China, in 2010 and 2015, respectively.

From 2015 to 2016, he was a Power System Engineer with the State Grid Sichuan Electric Power Research Institute, Chengdu, China. From December 2017 to December 2018, he was a Visiting Professor with the Department of Energy Technology, Aalborg University, Aalborg, Denmark. From 2017 to 2019, he was an Assistant Professor with the University of Electronic Science and Technology of China (UESTC). He is currently a Professor with the College of Electrical Engineering, Zhejiang University, Hangzhou. His research interests include high-voltage DC (HVDC) transmission, flexible AC transmission systems (FACTS), and DC distribution networks.

RUI YIN was born in Hengshui, China, in June 1990. He received the B.E. degree in power system and its automation from North China Electric Power University, Baoding, China, in 2012, and the Ph.D. degree in electrical engineering from Zhejiang University, Hangzhou, China, in 2017.

He is currently an Engineer with State Grid Hebei Electric Power Company, Ltd., Shijiazhuang, China. His current research interests include renewable energy generation systems, HVDC, and smart grids.

ZHENGXU HE was born in Fuquan, China, in October 1990. She received the B.E. and M.Eng. degrees in environmental engineering from Tsinghua University, Beijing, China, in 2012 and 2015, respectively.

She is currently a Researcher with the Sichuan Energy Internet Research Institute. Her research interests mainly include building energy efficiency, the energy internet, and the Internet of Things.

CONGLING WANG received the B.S. degree from the Nanjing University of Aeronautics and Astronautics, Nanjing, China, in 1991, and the M.S. degree from the University of Electronic Science and Technology of China (UESTC), Chengdu, China, in 1996. Since 1996, he has been a Faculty Member with the School of Mechatronics Engineering. He is currently an Associate Professor with UESTC. His research interests include mechatronics engineering, electrical engineering and automation, computer-aided control and instrumentation, smart mechatronics, and detection and automation of mechanical equipment.